LEEM investigations of ion beam effects on clean metal surfaces: quantitative studies of the driven steady state

2009 J. Phys.: Condens. Matter 21 314021

(http://iopscience.iop.org/0953-8984/21/31/314021)

IOP Publishing Journal of Physics: Condensed Matter

J. Phys.: Condens. Matter **21** (2009) 314021 (10pp) doi:10.1088/0953-8984/21/31/314021

LEEM investigations of ion beam effects on clean metal surfaces: quantitative studies of the driven steady state

Wacek Swiech[1], **Michal Ondrejcek**[2] **and C Peter Flynn**

Physics Department and Frederick Seitz Materials Research Laboratory, University of Illinois at Urbana-Champaign, Urbana, IL 61801, USA

E-mail: wswiech@illinois.edu

Received 30 December 2008, in final form 11 March 2009
Published 7 July 2009
Online at stacks.iop.org/JPhysCM/21/314021

Abstract

The technique of low-energy electron microscopy (LEEM) pioneered by Bauer has been adapted here to the investigation of ion beam processes on crystal surfaces by the incorporation of an intense and tunable source of selectable, energetic ions into a LEEM designed by Tromp *et al*. In this paper we explain principles that constrain the design of this tandem instrument, to permit observation of surfaces during irradiation. We also describe experiments that probe the driven steady state of surfaces subject to the perturbation of a uniform and constant flux of self-ions. The emphasis is on the example of Pt^- ions irradiating the Pt(111) surface. We explore a regime of linear response at elevated temperature in which the driven nucleation and universal driven growth of surface islands, and the driven cycling of Bardeen–Herring sources and other surface clocks, may be understood in a fully quantitative manner.

1. Introduction

Bauer and his collaborators not only developed the low-energy electron microscope as a preeminent tool for surface microscopy, but also employed the instrument for pioneering investigations in almost all areas of surface science on which subsequent work has focused [1–12]. These include surface doping and growth [13–17]; sublimation [18], surface reactions [19] and reconstructions [20–22]; structure and kinetics of boundaries among surface phases [18, 23, 24]; the evolution of surface micro-topography defined by step structure [18, 25–27]; and the behavior of surface magnetism [28–32]. It is towards a recognition of his major contributions to this field that the present paper is dedicated.

The topic addressed here is the application of LEEM to the *in situ* investigation of surfaces that are driven from equilibrium by irradiation, using a beam of energetic ions. A feature new to LEEM research is the incorporation into a LEEM of an intense beam of energetic self-ions that permits observation in real time of surface response to the disturbance caused by the ion beam. Ion beams cause complicated modifications of surfaces that depend on the energy and chemical identity of the perturbing ions, and also on their direction [33–37]. Incident ions of sufficiently low energy add material to a crystal, while ions above a 'neutral' energy ε_0 cause a net loss of material by sputtering. At sufficiently low ambient temperatures an ion beam can cause a surface to disorder and even become amorphous. These complex effects vary from one surface orientation to the next, even for a given crystal. Quantitative understanding of surface evolution has been achieved in few, if any, practical cases. This rich variety of accessible surface phenomena amply justifies efforts to explore their character afresh using the established power of low-energy electron microscopy.

With these complications in mind, a significant part of our effort has been spent on the simplification of the phenomena for the purpose of rendering them comprehensible in quantitative terms. Four particular simplifications have run through the breadth of our research. These are: (1) the use of self-ions to eliminate chemical reactions; (2) the use of elevated temperatures at which the diffusion processes on a surface respond to the ion beam to create a driven steady state that can be probed using LEEM; (3) a limitation to the regime of modest perturbations, in which the response of the surface

[1] Author to whom any correspondence should be addressed.

[2] Present address: National Center for Supercomputing Applications, University of Illinois at Urbana-Champaign, Urbana, IL 61801, USA.

to the driving force is linear [38]; and (4) the use of simplified surface conditions under which the complex response to local surface nanotopography is carefully controlled [39]. These four topics are amplified in the brief remarks that follow.

It must be understood that even a simple surface, almost flat, supports a complex of processes at elevated temperatures. Adatom–advacancy pairs form and annihilate spontaneously on open terraces. These species of thermal point defect are each created and annihilated continually also at step edges [40]. Together these processes establish equilibrium densities of point defects on the terraces, and the defects are in turn responsible for the transport of matter over the surface by diffusion [41]. The surface mass diffusion coefficient can be determined accurately from the resulting fluctuations of the step profiles, using 'step fluctuation spectroscopy' with video sequences obtained by LEEM [42–51]. In this dynamic equilibrium, foreign ions create a formidable complication. They alter the energetics of defect formation and diffusion, and change step edge stiffnesses and fluctuation amplitudes, all in imperfectly predictable ways. Such processes are inevitable when a surface is irradiated with foreign ions. In contrast, a beam of self-ions causes no chemical complications. At low impact energies a beam of self-ions adds host atoms to the surface, while at high energies there is a net loss of host atoms by sputtering. The desire to avoid chemical complication of the surface mixing has confined our initial investigations to processes that employ only beams of self-ions.

A second important simplification takes place at high temperatures where the surface mixing (measured by the surface mass diffusion coefficient) is rapid. The critical point here is that fast diffusion causes rapid healing of the damage from the impact of energetic ions. Each ion impact creates numerous adatom–advacancy pairs, in addition to bulk vacancies and interstitials, together with a local 'thermal spike', which however cools rapidly in a period of some picoseconds. The conceptually simple regime occurs when the resulting excess of thermal defects, both surface and bulk, disappears rapidly by reaction both with each other and at extended defects (surfaces, damage sites, step edges, etc) [52, 53]. When recombination is complete the net effect of a beam of self-ions with energy less than ε_0 is just to inject excess adatoms onto a surface, thereby perturbing the dynamic equilibrium of surface defect reaction in a way which is, at least in principle, capable of accurate discussion. Similarly, the net effect of a beam of self-ions with energy greater than ε_0, so that a net sputtering of ions takes place each impact, is to inject a net excess of advacancies onto the surface, with comparably tractable consequences. For this simplified context we refer in what follows to the beams in these two categories as an 'adatom beam' and an 'advacancy beam', respectively.

A third, equally necessary, restriction is to the use of weak beams for which the response of the surface to the ion beam perturbation is linear in the ion beam flux. As equilibrium is determined in part by reaction among antidefects, the equations that determine beam-induced perturbations are certainly nonlinear, and in fact the nonlinear terms prove dominant at the high temperatures of the present investigations. Specifically, the lifecycle of thermal antidefects under the conditions of our experiments are dominated by the pair processes of spontaneous creation and annihilation, rather than by events for adatoms and advacancies separately at step edges or other sinks. It is nevertheless always the case that processes close to equilibrium respond linearly to small perturbations and can be expressed in terms of linear hydrodynamic equations for diffusion, etc, with well-defined flow parameters such as equilibrium diffusion coefficients. By confining the present research to this regime it becomes possible to describe and interpret the results quantitatively using the theory of linear response [38].

Simplification of the material surface employed in experiments is also essential to reproducible surface response. Defect reactions, and hence also irradiation effects, are sensitive to the defect sinks associated with surface steps. Uncontrolled variations of surface step configurations therefore present major geometrical complications in the interpretation of surface response (as a crude illustration of this critical factor, the change of defect density depends on the square of the step spacing). To gain control of this experimental problem we have devised means, using the self-ion beam, for creating large, approximately round, arenas formed by perfect surface terraces [39]. These are isolated from the surrounding surface structure by a peripheral step bunch. Bunches of steps pointed outward create 'mesas' isolated above the surrounding surface, while bunched steps pointing inward create 'pans' isolated below their surroundings. The step bunches isolate driven processes inside these arenas from any perturbation of chemical potential caused by steps exterior to the step bunch. An example of such a mesa is shown in figure 1. In our research, pans and mesas up to $\sim$10 μm in size have been synthesized by ion beam methods, as explained in detail elsewhere [39]. For the applications discussed in this paper, pans and mesas provide ideally simplified surface conditions under which fundamental investigations of surface response to the driving force of ion beam irradiation may be undertaken.

In what follows we provide, in section 2, practical information about the LEEM–ion beam tandem and its use in experiments. Results for driven processes on pans and mesas are described in section 3. Some introductory comment about the theoretical framework that underpins the interpretation is also provided.

2. Experimental matters

Here we first recount in section 2.1 the design principles and some practical details pertinent to the LEEM–ion beam tandem, and then in section 2.2 explain its practical use.

2.1. The LEEM–ion beam tandem

While ions with high energies, up to $\sim$50 keV, are of technical value for implantation doping, particularly for semiconductor materials, much smaller ion energies are of principal interest for surface processes. The neutral energy for metal surfaces is typically $\sim$200 eV [52]; self-ion impacts of larger energy produce net loss of host atoms from a surface by sputtering,

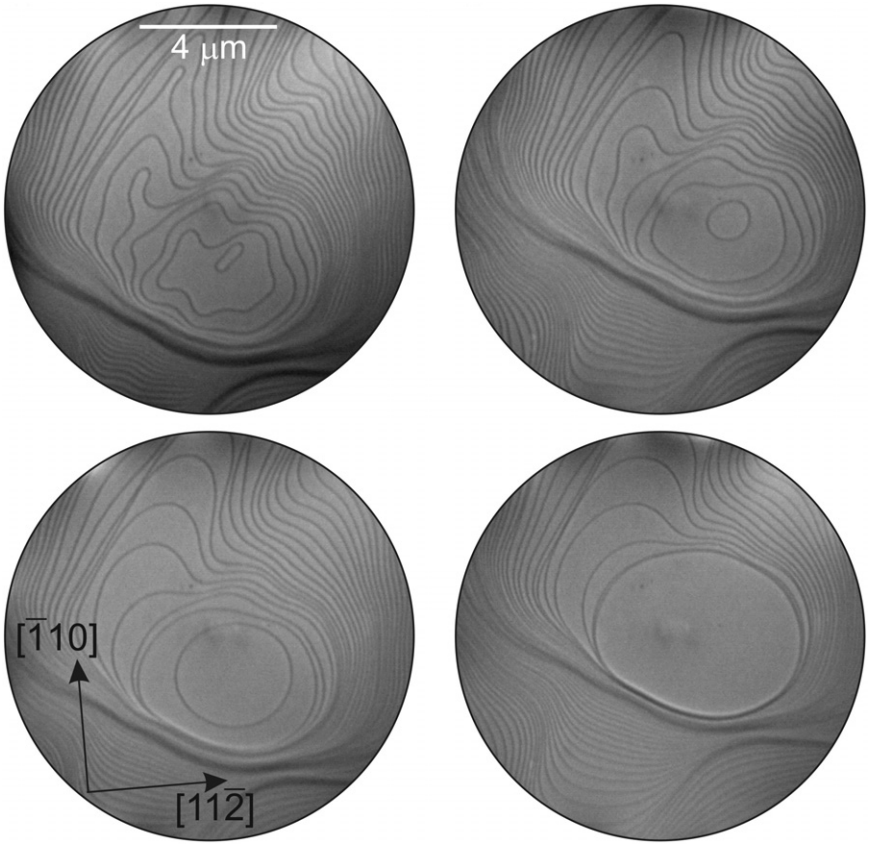

Figure 1. LEEM micrographs showing the evolution of a mesa from a local surface maximum on Pt(111) under irradiation by 4.6 μA cm^{-2} of 65 eV Pt$^-$ ions at 1190 K. The initial structure exhibits step geometries shaped by earlier processes of screw dislocation slip. The (adatom) ion beam causes the step contours to expand, with the inner islands overtaking the outer steps to create a step bunch surrounding a perfect raised terrace. The process can be continued, and the mesas expanded, as long as nucleation of a new island is avoided.

up to ∼10 atoms per impact for energies of several keV, while one ion per impact is, of course, added to the surface by a low-energy beam as the impact energy tends to zero. Interest for surface processes is mainly confined to energies ∼1 keV and below.

In conventional LEEM designs [9] the sample is at $\sim V_s = -15$ keV, in grounded surroundings. This renders impractical any proposed arrangement with positive ions for impacts of ∼1 keV; negative ions are thus essential. Also, as negative beams at grazing incidence must necessarily suffer large deflections, the use of negative ions at normal incidence and energy $>|V_s|$ becomes an attractive choice. In this scheme, the negative ions are decelerated from $15 + \varepsilon$ keV to the required low energies of ε keV by the sample potential. For our design, the source chosen for these negative ions was a SNICS II accelerator purchased from National Electrostatics Corp. [54–57] (with added differential pumping) to be integrated into a Tromp LEEM I [58]. It provided a beam of energy spread ∼65 eV FWHM, independent of mean energy [59]. The ion beam from the slits was relayed to a second focus near the sample by a 90° spherical deflector. It passed into the LEEM vacuum through the magnetic bending sector field, between the gun and imaging columns, and shared the electron path to the sample through a 1 mm hole in the objective lens. The lens was protected from the beam by a Ti tube that formed a beam dump, cooled by LN_2 from a Dewar, in order to efficiently re-condense unwanted sputtered material. A schematic diagram showing the main details is provided in figure 2 [59]. In operation the LEEM was used at sample temperatures up to 1700 K, with vacua $\sim 10^{-10}$ Torr, even with the ion source operational. Beam intensities varied up to ∼0.1 ML s, depending on the ion species, and could be monitored using the current to the beam dump. Absolute calibrations were made occasionally by measuring the LEEM sample current through the 1 mm aperture.

The space charge interaction between the electron beam and intense ion currents could cause the imaging capability of the LEEM to deteriorate at large ion beam currents [60]. This was accommodated when necessary by chopping the ion beam and monitoring the LEEM image only during the off period of the ion beam. By this method it was possible to monitor in real time (i.e. 30 video frames s^{-1}) the evolution, caused by the ion beam, of the undistorted LEEM image, up to the maximum available levels of irradiation.

2.2. *Experimental details*

The experiments described below require the best possible surface cleanliness. Some emphasis was therefore placed on sample preparation. As the results in section 3 concern the Pt(111) surface, we summarize here the procedures,

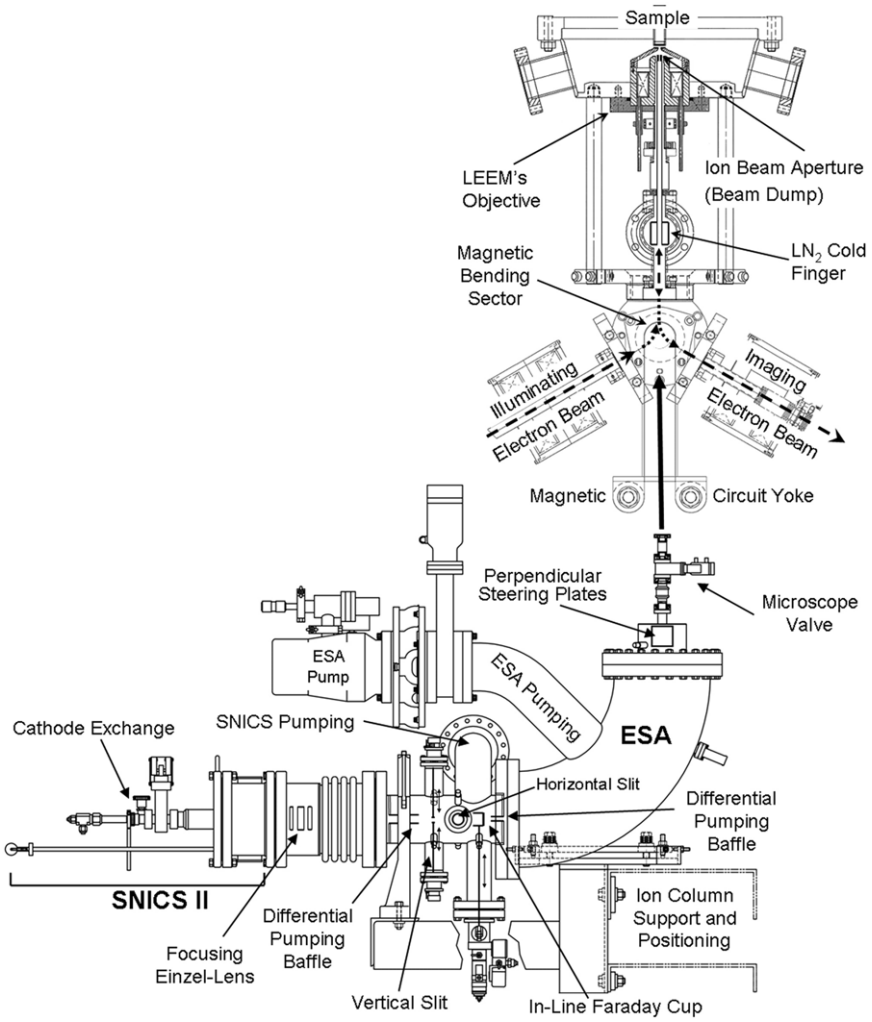

Figure 2. Sketch showing the SNICS II ion source configured so that the negative ion beam is relayed by an electrostatic spherical analyzer (ESA) to a focus near the LEEM sample [59]. The LEEM and SNICS II share a common vacuum, interconnected through the magnetic bending sector field chamber. Differential pumping introduced between the SNICS II and the ESA, together with the beam dump at LN_2 temperature in the LEEM anode space, maintained the 10^{-10} Torr vacuum capability of the LEEM.

as refined in this research, for the Pt(111) surface. The crystal employed in the work was purchased from the Surface Preparation Laboratory, The Netherlands. It was a single crystal of platinum, 9 mm in diameter and 0.8 mm thick, with a polished (111) front surface. The same crystal was used in earlier studies of mass diffusion by step fluctuation spectroscopy [44, 61]. Initially it was cycled repeatedly with 1 kV Ar^+ ion sputtering and 10^{-7} Torr O_2 exposure at 1100 K before introduction into the LEEM, where cleaning cycles were continued. The eventual surface exhibited sharp LEED reflections and no trace of impurity scattering or diffraction. The base vacuum for this work was in the low 10^{-11} Torr range, and the pressure remained at about 10^{-10} Torr for operating temperatures of 1300 K.

Large areas of the Pt surface with miscut $<0.1^\circ$ gave well-spaced and relatively straight step edges. In gross structure the crystal surface nevertheless contained minor minima and maxima spaced by $\sim$10's of μm, and these provided the loci for the initial preparation of pans or mesas, respectively, using the ion beam as described in a detailed report [39]. Once a suitable arena was grown, the effort was redirected to the specific experiments of the type described in section 3 below.

3. Quantitative experiments on driven surfaces

Three distinct types of experiment are described. First, the ion beam could be employed to raise or lower the chemical potential on the arena until an island nucleated near the center of the pan or mesa [53]. This work is described in section 3.1. Second, various beam strengths and energies could be employed to make islands grow or shrink. We find in our studies that these processes share a time evolution that has a universal form that agrees with new theoretical predictions [62]. The work is described in section 3.2. Finally, active structures other than islands may be captured on an arena and their operation under the driving force of an ion beam examined. The case of a Bardeen–Herring source is

described in section 3.3. Structures of this type act as 'clocks' that determine the net change of crystal volume caused by ion irradiation. For these structures, as for islands, the observations determine the net addition (or loss) of host atoms per ion at any particular impact energy, and this valuable calibration of surface response now becomes available for the interpretation of driven processes and for comparison with the predictions of molecular dynamics (MD) simulations [63].

The discussion of experimental observations in what follows is made possible by a general theory of linear surface response to ion beam irradiation [38], about which further remarks are offered as appropriate throughout the text.

3.1. Driven nucleation of adatom and advacancy islands

An adatom beam (i.e. $\varepsilon < 250$ eV) of self-ions on Pt(111) naturally raises the chemical potential μ^* of an irradiated arena and establishes a defect distribution in which the steady state chemical potential $\mu^*(\mathbf{r})$ depends on position $\mathbf{r}$. The boundary conditions at the peripheral step bunch maintain $\mu^* = 0$ there, so μ^* rises to a maximum near the center of the arena at $\mathbf{r} = 0$. (Here we recognize that the Gibbs–Thompson effect is negligible in the present range of measurements. The critical radius for nucleation is a few Ångströms, and this is where the driving force of irradiation balances the Gibbs–Thompson potential. For the larger radii observed here, the Gibbs–Thompson effect is reduced, in the ratio of the radii, by some orders of magnitude, below the driving force of the irradiation.) In the converse case of an advacancy beam ($\varepsilon > 250$ eV) the chemical potential is lowered throughout, and with a negative extremum near $\mathbf{r} = 0$. With increased beam intensity of either type the chemical potential μ^* increases proportionately (in linear response) until, for a sufficiently intense beam, μ^* exceeds the critical value μ_c^* at which an island is nucleated. This happens first near the center of the arena, where adatom beams nucleate adatom islands and advacancy beams nucleate advacancy islands. In either case, the island nucleation can be observed in real time by LEEM during actual irradiation. We thus acquire a method by which the conditions under which the nucleation of precipitates by an irradiating beam of either sign of antidefect can, for the first time, be examined under tightly controlled conditions, for comparison with the predictions of fundamental theory.

Some discussion is needed of the theoretical framework inside which the driven steady state on the terrace prior to nucleation can be treated [38]. The theory augments the diffusion equations for the adatoms, site occupancy c_1, and advacancies, site occupancy c_2, first by pair reaction terms $K_{12}(\bar{c}_1\bar{c}_2 - c_1c_2)$, in which $\bar{c}_1, \bar{c}_2$ are thermal equilibrium values, and second by beam production rates per site for the two antidefects, specifically K_1 and K_2. When linearized about the equilibrium condition the resulting equations can be solved generally for the static linear response to the ion beam terms K_1 and K_2. For a uniformly driven system, the steady state in which the defects react on an arena, and the excess diffuses in two dimensions to the peripheral step bunch leading to a time-independent distribution, is associated with an excess chemical potential [53]:

$$\mu^*(\mathbf{r}) = \frac{k_B T(K_1 - K_2)}{4(D_1\bar{c}_1 + D_2\bar{c}_2)}[R^2 - r^2]. \quad (1)$$

This falls to zero as required when r reaches the radius R of the step bunch at the boundary of the arena. Here, $D_1\bar{c}_1 + D_2\bar{c}_2 = D_s$ is the surface mass diffusion coefficient and $K_1 - K_2 = \Delta K$, linearly proportional to beam intensity, is the excess rate per surface site of adatom creation over advacancy creation by the ion beam. Both are known from experiments discussed later, the former from step fluctuation spectroscopy [45, 46] and the latter from calibration experiments that observe the motion of surface clocks (see below). Thus the value of μ^* near $r = 0$ is known from equation (1) for any given value of the ion beam intensity (and hence of ΔK). Experiments in which the ion beam intensity is slowly raised until nucleation is observed by LEEM thus determine, for comparison with fundamental theory, the critical chemical potential μ_c^* required to cause nucleation [53].

The chemical potential μ^* in this discussion is the value for the assembly of reacting antidefects. The separate antidefects have opposite chemical potentials because the addition of an adatom has precisely the same effect on the reacting assembly as the removal of an advacancy, and vice versa. As a consequence of this symmetry, the chemical potentials at which adatoms and advacancies nucleate are predicted to have the same magnitudes but opposite signs. Any discussion of the two species precipitating independently would arrive at a different prediction, with distinct values of μ_c^* that depend individually on the energetics of the two species of defect.

In practical experiments the method just outlined has been performed over a range of temperatures from 750 to 1260 K. As made apparent by figure 3, the observed μ_c^* scatter about a systematic variation through this range [53]. Three significant observations can be made from the data. First, throughout the range of results it is experimentally verified that the values of chemical potential required for the nucleation of adatom and advacancy islands are of equal magnitude but opposite sign. The prediction thus confirmed was based on linear response but needed, in addition, a simplified description of the island energetics in terms of step energies, which from the results also appears sufficiently valid. Second, $\mu_c^*/k_BT \ll 1$ in the range $970\ \text{K} < T < 1260\ \text{K}$. This critical finding means that the perturbation required for nucleation is small, so that the linear response theory, on which the interpretation is based, is in fact valid. It is also of interest that the values for $T < 970$ K do not satisfy this requirement so the interpretation is not valid there (see below). Finally, the dotted line in figure 3 that falls below the experimental points is the absolute prediction of μ_c^*, consistent with measured values of the step stiffness $\tilde{\beta}$, using the theory of nucleation for two-dimensional structures such as islands developed by Pimpinelli and Villain [64]. The predicted μ_c^* resembles that observed but evidently identifies values that are somewhat too small. The reasons that underlie this inaccuracy of the theory have not yet been identified.

For temperatures above about 1060 K, the available ion beam intensity falls short of the value required for nucleation

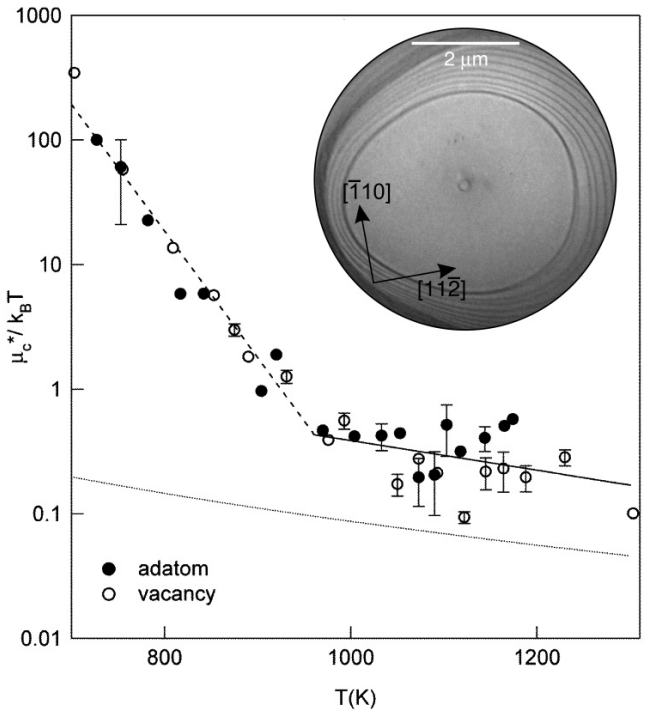

Figure 3. The inset is a LEEM micrograph of an island freshly nucleated on a pan. The data below show as functions of temperature the scaled chemical potentials μ_c^*/k_BT at which adatom islands (solid points) and advacancy islands (open circles) are seen to nucleate under the driving force of ion irradiation [53]. At temperatures above about 970 K, $\mu_c^*/k_BT \ll 1$. Thus the linear response theory employed to interpret the result is valid. The observations nevertheless differ from theoretical predictions of Pimpinelli and Villain (broken line) [64]. Below 970 K the data are in error, as the kinetics are slow, and the experiments allowed too little time to observe nucleation. Note that the common behavior of adatom and advacancy data confirm an earlier prediction.

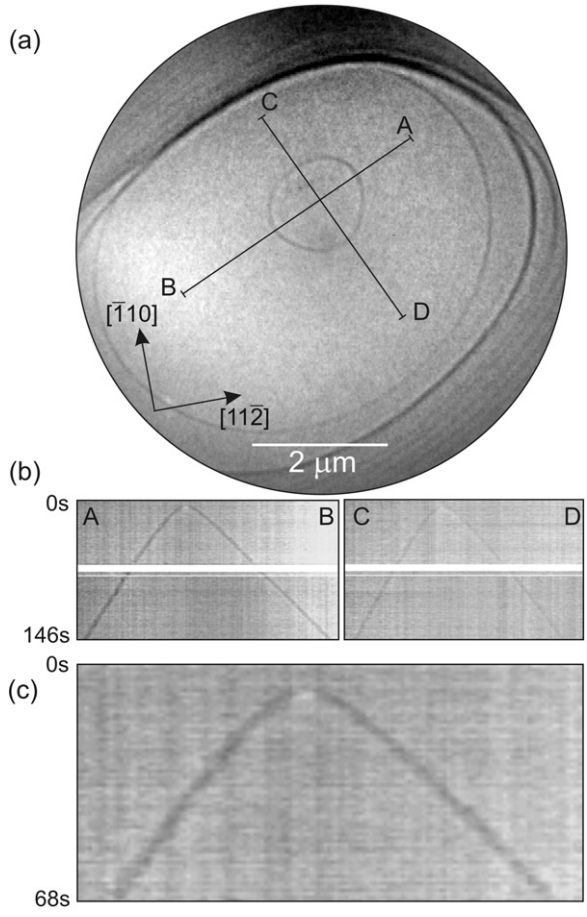

Figure 4. Island growth at small radii [62]. In (a), two diameters of an adatom island on a mesa on Pt(111) are defined. Pixel rows along these diameters in (rotated) images are shown displaced by time to reveal the dependence of diameter on time as an island nucleates and grows. The rounding as $a \to 0$ is confirmed in the enlarged image (b).

and no islands could form. In the opposite limit of low temperatures, the surface kinetics slow down so that islands are unable to nucleate and grow to observable size in the time allotted to the experiments. Apparently what evolved in practice was a surface overdriven by excessive irradiation so that many islands nucleated, spread over the arena. The values of μ_c^*/k_BT acquired below 970 K are larger than unity, so their interpretation in terms of linear response theory is itself also not valid. It is of interest that the data for adatom and advacancy islands nevertheless define conditions that still reflect a symmetry between the two distinct processes. Much more research on Pt(111) and other systems is needed before these important process can become better understood.

3.2. Universality in the driven growth of islands

Once an island has nucleated, the new defect sink formed by its step edge alters the distribution $\mu_c^*(r)$ near its radius a such that $\mu_c^*(a) = 0$. Excess defects created by the ion beam then precipitate at the step at a in addition to the step bunch at the perimeter of the arena at R. As a result, the island grows, provided that the sign of the beam remains unchanged (it shrinks if adatom and advacancy beams are interchanged). From LEEM video sequences we have tracked both the growth and shrinking for a variety of adatom and advacancy islands isolated on pans and mesas. We find, to a good approximation, that the observed growth follows a universal form, particularly when the radius is half or less that of the arena.

As an experimental matter some variability at larger a appears to arise from the way islands typically do not nucleate exactly at the center of the arena, so that different cases have slightly different diffusion geometries as the island grows out to the surrounding step bunch. In earlier research it had been thought that islands grow linearly in time, but that is not precisely the case [52, 65, 66]. Both in growth and shrinkage the rate of change is larger at small radii. We shall see that the theory predicts a behavior that is non-analytical as $a \to 0$, and the experiments closely agree with the predicted form.

To give a flavor of the results, figure 4(a) defines diameters of an island, chosen to represent its size. Note the weak threefold character of island shape from anisotropy of the step energy; this inverts as expected between adatom and advacancy islands [62]. Figure 4(b) shows pixel rows displaced vertically in proportion to time lapse so that the diameter as a function of time is revealed by video intensity changes. The time evolution

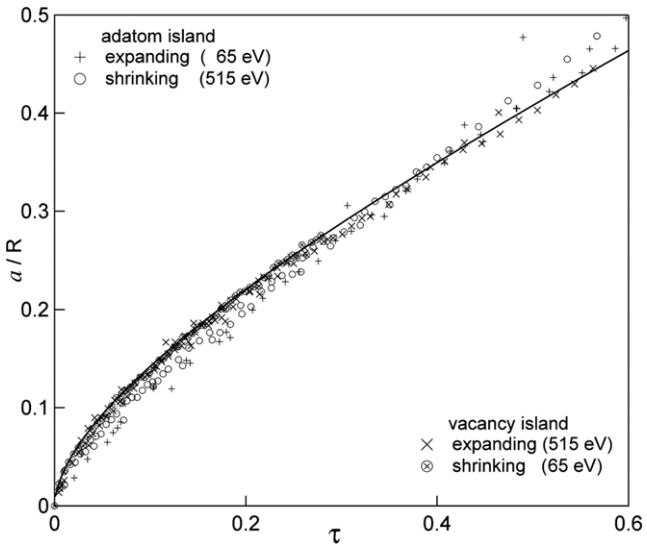

Figure 5. Universality of island growth on Pt(111) is demonstrated by the superposed data points that record the growth and shrinking of both adatom and advacancy islands [62]. The universal prediction of the theory from equation (3) is indicated by the solid line near the data. In the theory, the variations as x → 1 (i.e. $a \to 0$) is not analytical owing to the capture by the island step edge of defects from irradiation events outside the island.

of each diameter clearly indicates a nonlinear rounding as the radius $a \to 0$.

These matters are fully quantified in figure 5, in which the observed time evolution is shown for a variety of cases for both adatom and advacancy islands, both in growth and shrinking processes (with the latter shown time reversed) [62]. The solid line is the behavior predicted by the theory, discussed below. It is apparent that the different cases do indeed have very similar time evolutions.

In treating the behavior quantitatively, the limit of quasistatic behavior for a linearly responding system in two dimensions is invoked. The quasistatic profile is [38, 52]

$$\mu^*(r) = \frac{k_B T(K_2 - K_1)}{4(D_1\bar{c}_1 + D_2\bar{c}_2)}[r^2 - a^2], \qquad (r < a). \quad (2a)$$

For $a < r < R$, on the terrace outside the island, the solution is

$$\mu^*(r) = \frac{k_B T(K_2 - K_1)}{4(D_1\bar{c}_1 + D_2\bar{c}_2)}\left[r^2 - R^2 - \frac{(a^2 - R^2)\ln(r/R)}{\ln(a/R)}\right]. \quad (2b)$$

In this description, the division of precipitating defects between the island step and the peripheral step bunch has a purely geometrical dependence on the ratio a/R of the radii, and it is this property that renders the behavior universal. In an exact solution, the flow due to creation of excess defects by irradiation is very much larger than any flow caused by island growth and consequent changes of boundary conditions on the reacting assembly of defects; the quasistatic approximation is therefore valuable. The flux J to the island is obtained from the Nernst–Einstein equation, and the rate of step advance for an adatom island with an adatom beam obtained from the area A added per precipitated adatom as $\mathrm{d}a/\mathrm{d}t = J(a)A$ or, from equations (2) [62]:

$$\frac{\mathrm{d}x}{\mathrm{d}\tau} = \frac{(x^2 - 1)}{x \ln x}; \qquad x = a/R; \quad \tau = (\Delta K/4)t, \quad (3)$$

in which $\Delta K = K_1 - K_2$ as above and the solution is valid for $0 < x < 1$.

The scaled form of equation (3) clearly reveals the predicted universality. At $x = 0$ the derivative diverges and the solution is not analytical. It may be expressed as a power series multiplying $x^2 \ln x$, and related to the logarithmic integral $\mathrm{li}(x)$. Neither the pathway nor the absolute rate of island evolution predicted by equation (3) depends on the diffusion coefficients of the mobile thermal point defects responsible for the surface transport that drives the growth process. The steady state defect concentrations built up by irradiation rise to levels inversely proportional to the diffusion coefficient, which therefore cancels from the flux $\sim D\nabla c$. Then in this steady state, the net flux to the steps exactly equals the net creation rate of defects, independent of diffusion rates. It may finally be noted that, at small island radii for which $x \to 0$, the flux to the island itself arises disproportionately from irradiation events that occur outside the island.

For the present purposes, the point of greatest interest is a comparison between the observed island growth and the universal form predicted by the quasistatic theory. For this purpose, the solid line passing among the experimental values in figure 5 above represents the solution of equation (3) from the theory. The theory provides an adequate description of the observed rates of driven island evolution for the range of radii represented there. As mentioned earlier, deviations from universality often occur for still larger radii, particularly for off-center or non-circular islands.

3.3. Driven surface clocks

Certain surface structures respond with sufficient regularity under the driving force of irradiation that they may well, for future purposes, be termed 'surface clocks'. They have periods that depend linearly on the irradiation flux and find utility by providing a means for calibrating the effect, per incident ion, of the irradiation on the surface. Specifically, they determine the value of $\Delta K = K_1 - K_2$ quantitatively. A brief introduction to the topic is offered here.

It has long been recognized that, when a screw dislocation intersects a free surface, the intersection is marked by the termination of a surface step. The fact that a driving force such as vapor growth or sublimation at elevated temperatures causes the step to evolve into a shape closely resembling an Archimedean spiral played an important part in early efforts to understand the mechanisms of crystal growth [67]. It is readily perceived that any process that adds or subtracts atoms layer by layer must cause such a structure to rotate precisely through 2π for each layer, in order that the configuration is exactly reproduced in each atomic layer. For this reason the spiral may be regarded as a clock that records the loss or gain of atomic layers. A slightly more elaborate clock is formed when a length of step edge begins and ends at two neighboring

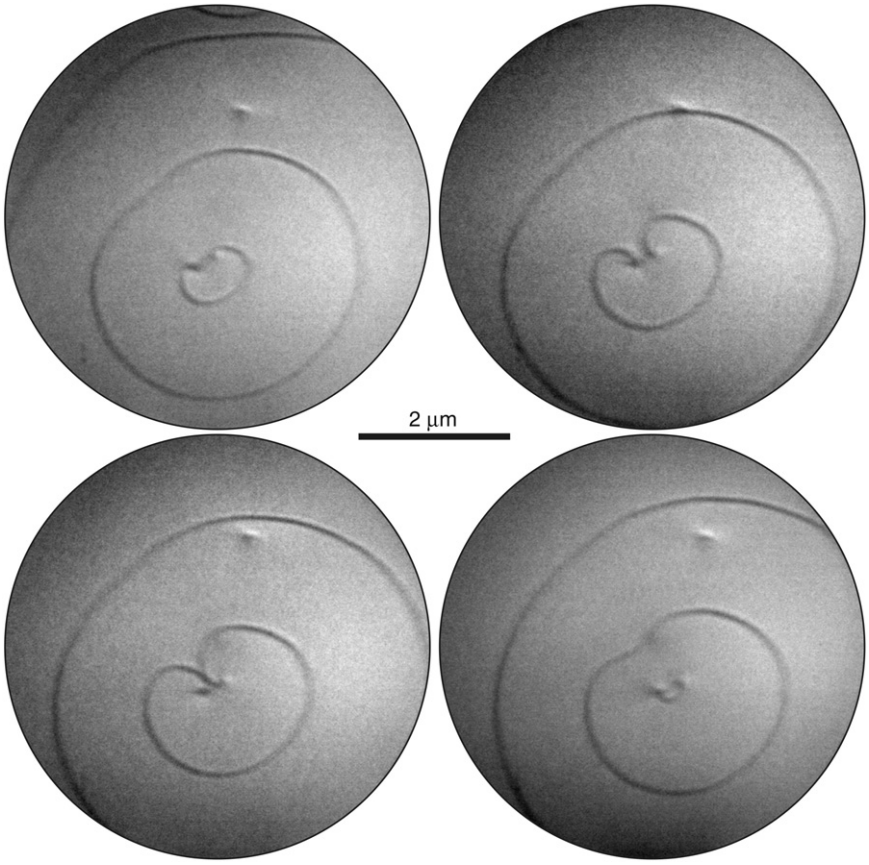

Figure 6. The cycling of a Bardeen–Herring source under irradiation by an adatom beam of 515 eV Pt^- ions at ∼960 K on Pt(111). The inner step extends between two screw dislocations of opposite sign, made visible by local contrast from their surface strain fields (top left). The pressure of irradiation-driven adatoms causes the inner step edge to bow out (top right) and eventually self-intersect (bottom left). This spins off a new complete island loop and leaves behind a new length of step connecting the two screws (bottom right).

screw dislocations of opposite sign [66, 68]. Step edge climb driven by excess defects of either sign causes the step to bow and eventually self-intersect to form an island that surrounds the dislocations. This acts to create new islands at regular time intervals, much as slip of a Frank–Reed source [69] creates dislocation loops in the bulk. To distinguish the two cases we term the process with climb at a surface a Bardeen–Herring source [70] and reserve the term Frank–Reed source for the case of slip. The Bardeen–Herring source forms a precise surface clock that cycles under irradiation exactly once each monolayer added or subtracted.

An example of Bardeen–Herring sources observed in our research on Pt(111) is shown in figure 6. We have verified that such sources cycle as predicted under irradiation. It may be noted that the universal island growth described above also constitutes a clock of sorts, since its growth period from $a = 0$ to R depends only on ΔK.

The dependence of these clock periods on ΔK affords a convenient method by which ΔK may be determined by LEEM observation with an *in situ* ion source. To this end we have verified that the periods of the three types of clock described here are in agreement, within the uncertainty of ∼10% of the absolute flux reproducibility of the SNICS II source. Figure 7 shows values of ΔK determined from surface clocks [52]. There, the results are compared with the absolute MD predictions for Pt ions of various energies impacting on Pt(111) in the molecular dynamics calculations of Averback and co-workers [63]. There is good agreement between the two, which establishes in addition that the MD calculations are very effective, even at the low impact energies pertinent to the present research.

4. Summarizing comments

Since their invention and development by Bauer, LEEM and PEEM have blossomed to take their place among the most important tools of surface science, with diverse applications in areas such as chemistry, synchrotron radiation and magnetism far outside the locus of the initial research. In this paper we describe yet a further new application of LEEM observations in real time to explore the driving effects of self-ion irradiation on clean metal surfaces. It is our expectation that new applications for this valuable research tool will continue to open up for some considerable time to come.

Acknowledgments

This research was funded in part by the DOE through grants DE-FG02-08ER46549 and DEFG02-02-ER46011. The LEEM

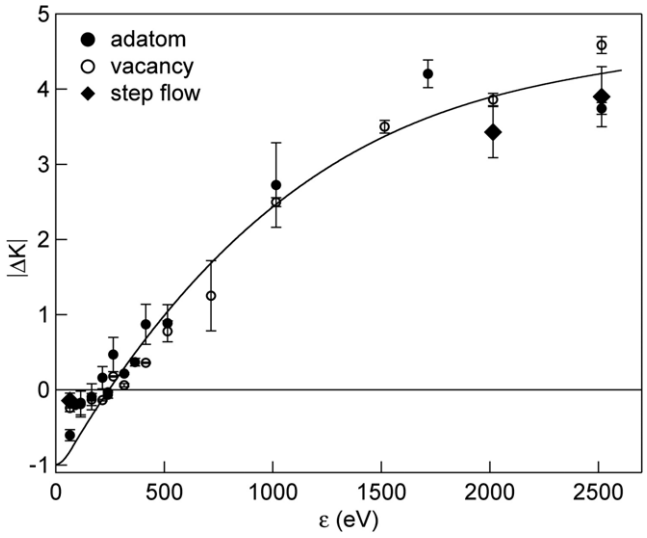

Figure 7. A calibration of the additional surface atoms per incident self-ion obtained from studies of island growth rates for Pt^- ion irradiation at the energies shown by data points [52]. Diamonds indicate data obtained instead from the driven motion of straight steps. The 'neutral' energy at which exactly one ion sputters from the surface per incident ion, leaving no net change, is about 250 eV. The solid line interpolates among results calculated for Pt(111) by Averback and co-workers using molecular dynamics calculations that include sample temperature [63]. Evidently the MD results are able to give satisfactory predictions for these surface processes at low impact energies.

was maintained in the Center for Microanalysis of Materials of the University of Illinois Frederick Seitz Materials Research Laboratory, funded in part by grant DEFG02-91-ER45439.

References

[1] Bauer E 1962 *Electron Microscopy* vol 1 (New York: Academic) p D-11
[2] Turner G H and Bauer E 1966 *Electron Microscopy* vol 1 (Tokyo: Maruzen) p 163
[3] Bauer E 1978 *Leopoldina Symp. on Physik und Chemie der Kristalloberflaeche (Halle, DDR)* unpublished
[4] Telieps W 1983 *PhD Thesis* Technische Universitaet Clausthal
[5] Telieps W and Bauer E 1985 *Ultramicroscopy* **17** 57
[6] Bauer E and Telieps W 1988 *Surface and Interface Characterization by Electron Optical Methods* (New York: Plenum) p 195
[7] Veneklasen L H 1991 *Ultramicroscopy* **36** 76
[8] Veneklasen L H 1992 *Rev. Sci. Instrum.* **63** 5513
[9] Bauer E 1994 *Rep. Prog. Phys.* **57** 895
[10] Bauer E, Franz T, Koziol C, Lilienkamp G and Schmidt Th 1997 *Chemical, Structural and Electronic Analysis of Heterogeneous Surfaces on the Nanometre Scale* (Dordrecht: Kluwer) p 75
[11] Bauer E, Koziol C, Lilienkamp G and Schmidt Th 1997 *J. Electron Spectrosc. Relat. Phenom.* **84** 201
[12] Bauer E 1998 *Surf. Rev. Lett.* **5** 1275
[13] Bauer E 1994 *Scanning Microsc.* **8** 765
[14] Bauer E 1996 *Appl. Surf. Sci.* **92** 20
[15] Schmidt Th and Bauer E 2000 *Phys. Rev.* B **62** 15815
[16] Schmidt Th and Bauer E 2001 *Surf. Sci.* **480** 137
[17] Jalochowski M and Bauer E 2001 *Surf. Sci.* **480** 109
[18] Mundschau M, Bauer E, Telieps W and Swiech W 1989 *Surf. Sci.* **223** 413
[19] Schmidt Th, Schaak A, Guenther S, Ressel B, Bauer E and Imbihl R 2000 *Chem. Phys. Lett.* **318** 549
[20] Altman M S and Bauer E 1995 *Surf. Sci.* **344** 51
[21] Altman M S and Bauer E 1996 *Surf. Sci.* **347** 265
[22] Pavlovska A and Bauer E 2005 *Surf. Interface Anal.* **37** 110
[23] Mundschau M, Bauer E and Swiech W 1988 *Catal. Lett.* **1** 405
[24] Atala P, Phaneuf R J, Bartelt N C, Swiech W and Bauer E 1995 *Mater. Res. Soc. Symp. Proc.* **404** 117
[25] Bauer E 1995 *Phys. Status Solidi* b **192** 375
[26] Meyer zu Heringdorf F-J, Kaehler D, Horn-von Hoegen M, Schmidt Th, Bauer E, Copel M and Minoda H 1998 *Surf. Rev. Lett.* **5** 1167
[27] Meyer zu Heringdorf F-J, Hild R, Zahl P, Schmidt Th, Ressel B, Heun S, Bauer E and Horn-von Hoegen 2001 *Surf. Sci.* **480** 103
[28] Altman M S, Pinkvos H, Hurst J, Marx G and Bauer E 1991 *Mater. Res. Soc. Symp. Proc.* **232** 125
[29] Duden Th and Bauer E 1995 *Rev. Sci. Instrum.* **66** 2861
[30] Bauer E 1997 *Handbook of Microscopy* (Weinheim: VCH) p 751
[31] Duden Th and Bauer E 1998 *Surf. Rev. Lett.* **5** 1213
[32] Bauer E 2001 *AIP Conf. Proc.* **570** 965
[33] Averback R S and de la Rubia T D 1998 *Solid State Physics* vol 51, ed H Ehrenreich and F Spaepen (New York: Academic) p 281
[34] Chason E, Picraux S T, Poate J M, Borland J O, Current M I, de la Rubia T D, Eaglesham D J, Holland O W, Law M E, Magee C W, Mayer J W, Melngailis J and Tasch A F 1997 *J. Appl. Phys.* **81** 6513
[35] Evans J W, Thiel P A and Bartelt M C 2006 *Surf. Sci. Rep.* **61** 1
[36] Michely T and Krug J 2004 *Islands, Mounds and Atoms* (Berlin: Springer)
[37] Mutaftschiev B 2001 *The Atomistic Nature of Crystal Growth* (Berlin: Springer)
[38] Flynn C P 2007 *Phys. Rev.* B **75** 134106
[39] Flynn C P, Ondrejcek M and Swiech W 2008 *J. Phys.: Condens. Matter* **20** 395001
[40] Flynn C P 2005 *Phys. Rev.* B **71** 085422
[41] Flynn C P 2006 *Phys. Rev.* B **73** 155417
[42] Flynn C P 2002 *Phys. Rev.* B **66** 155405
[43] Ondrejcek M, Swiech W, Durfee C S and Flynn C P 2003 *Surf. Sci.* **541** 31
[44] Ondrejcek M, Swiech W and Flynn C P 2004 *Surf. Sci.* **566–568** 160
[45] Ondrejcek M, Swiech W, Yang G and Flynn C P 2004 *Phil. Mag. Lett.* **84** 69
[46] Ondrejcek M, Swiech W, Rajappan M and Flynn C P 2005 *Phys. Rev.* B **72** 085422
[47] Ondrejcek M, Rajappan M, Swiech W and Flynn C P 2005 *Surf. Sci.* **574** 111
[48] Ondrejcek M, Rajappan M, Swiech W and Flynn C P 2006 *Phys. Rev.* B **73** 035418
[49] Ondrejcek M, Swiech W and Flynn C P 2006 *Phil. Mag.* **86** 1387
[50] Ondrejcek M, Swiech W and Flynn C P 2006 *Surf. Sci.* **600** 4673
[51] Ondrejcek M, Rajappan M, Swiech W and Flynn C P 2006 *J. Appl. Phys.* **100** 083523
[52] Rajappan M, Swiech W, Ondrejcek M and Flynn C P 2007 *Phil. Mag.* **87** 4501
[53] Flynn C P, Swiech W, Ondrejcek M and Rajappan M 2008 *Phys. Rev.* B **77** 045406
[54] Middleton R 1983 *Nucl. Instrum. Methods* **214** 139
[55] Rathmell R D 1986 *Rev. Sci. Instrum.* **57** 727
[56] Rathmell R D and Norton G A 1987 *Nucl. Instrum. Methods* B **21** 270
[57] Ferry J A, Loger R L, Norton G A and Raatz J E 1996 *Nucl. Instrum. Methods* A **382** 316
[58] Tromp R M and Reuter M C 1991 *Ultramicroscopy* **36** 99

[59] Swiech W, Rajappan M, Ondrejcek M, Sammann E, Burdin S, Petrov I and Flynn C P 2008 *Ultramicroscopy* **108** 646
[60] Larson J D 1986 *Nucl. Instrum. Methods Phys. Res.* A **244** 192
[61] Rajappan M, Swiech W, Ondrejcek M and Flynn C P 2007 *J. Phys.: Condens. Matter* **19** 226006
[62] Flynn C P, Swiech W and Ondrejcek M 2008 *Phys. Rev.* B **78** 075420
[63] Vo N Q, Krasnochtchekov P and Averback R S 2006 (UIUC) unpublished
[64] Pimpinelli A and Villain F 1994 *Physica* A **204** 521
[65] Metois J J and Wolf D E 1993 *Surf. Sci.* **298** 71
[66] Tang S J, Kodambaka S, Swiech W, Petrov I, Flynn C P and Chiang T C 2006 *Phys. Rev. Lett.* **96** 126106
[67] Nabarro F R N 1980 *Dislocations in Solids* vol 5 (Amsterdam: North-Holland)
[68] Kodambaka S, Israeli N, Bareno J, Swiech W, Ohmori K, Petrov I and Greene J E 2004 *Surf. Sci.* **560** 53
[69] Hirth J P and Lothe J 1982 *Theory of Dislocations* (New York: Wiley)
[70] Bardeen J and Herring C 1952 *Imperfections in Nearly Perfect Crystals* (New York: Wiley) p 261